In vitro cytotoxicity profiles of some polymers and inorganic nanoparticles commonly used in nanomedicine

Akshay Bugwandeen, Kerisha Singh, Aliscia Daniels, Dhireshan Singh, Lorenzo Lance David and Moganavelli Singh*

Nano-Gene and Drug Delivery Group, Discipline of Biochemistry, School of Life Sciences,
College of Agriculture, Engineering and Science, University of KwaZulu-Natal,
Private Bag X54001, Durban, 4000, South Africa.

ABSTRACT

With the advent of nanotechnology has come an array of nanomaterials that can be used in biomedical applications. Inorganic nanoparticles have therapeutic potential due to their favourable properties, including small size, ease of synthesis, and high surface-to-volume ratio. However, functionalization with cationic polymers is required to enhance their stability and allow for therapeutic agent conjugation. Due to the potential associated toxicities of some nanoparticles and polymers, their therapeutic use has been halted. Hence, the study at hand evaluated the *in vitro* cytotoxicity of popular inorganic nanoparticles (NPs) (gold, silver, selenium, and palladium) and cationic polymers (poly-L-lysine, polyethyleneimine, and chitosan) in four mammalian cell lines. All NPs were chemically synthesized and characterized using UV-visible spectroscopy. NPs and polymers were morphologically and physiochemically characterized with transmission electron microscopy (TEM) and nanoparticle tracking analysis (NTA), which revealed that both NPs and polymers were within the nanometre size range. There was evidence to support the instability of uncoated NPs and the highly stable and cationic nature of the polymers tested. Cytotoxicity revealed that gold and palladium NPs were well tolerated across all cell lines, with silver NPs exhibiting high levels of cell death.

*Corresponding author: singhm1@ukzn.ac.za

Selenium NPs showed selective cell death in the cancer cell lines, confirming the anticancer properties of these NPs. All polymers were well tolerated in the non-cancer cells but exhibited slight toxicity levels in the cancer cells. Overall, this *in vitro* cytotoxicity study provides valuable information that can assist in the way forward for using these nanoparticles and polymers in nanomedicine for cancer therapy.

KEYWORDS: nanomedicine, cancer therapy, inorganic nanoparticles, cationic polymers, *in vitro,* cytotoxicity.

INTRODUCTION

Cancer is one of the leading causes of mortality worldwide, with an increasing number of new cases and close to 10 million deaths annually [1, 2]. Conventional treatment methods include surgery, chemotherapy, and radiation. However, these methods have limitations such as non-specific drug distribution in the body, insufficient drug delivery to the tumour site, multi-drug resistance, and invasiveness of surgery. For successful cancer therapy, the therapeutic molecule must be delivered directly to the specific cancer cells while reducing damage to healthy cells [3].

Nanotechnology has attracted significant interest in therapy, with nanomedicine offering the exciting possibility of diagnostic imaging and cell-specific targeting [4]. Nanoparticles (NPs), in the 1-100 nm size range, exhibit several unique physical, biological,

chemical, and electronic properties [5]. The use of NPs offers several advantages over current treatment methods, which include their theranostic potential, ease of synthesis with a high carrying capacity, conjugation of targeting ligands for tumour cell specificity, the possibility of combinatorial therapy due to their ability to be conjugated with multiple drug molecules and the ability to overcome drug resistance mechanisms [3]. NPs such as gold (Au), silver (Ag), and selenium (Se) have exhibited anticancer and antioxidant properties in biological systems [6]. Gold nanoparticles (AuNPs), with their favourable physicochemical properties, have been among the most popular and versatile NP utilized in gene and drug delivery. They are known for their ease of synthesis, large surface area, biocompatibility, and unique optical properties [7, 8]. AgNPs have gained popularity in nanomedicine due to their optical, physical, chemical, and magnetic properties, which are largely dependent on their size and shape [9]. They have been utilized in biosensors, cosmetics, antimicrobials, nanocomposites, imaging, and filters [10]. Se has attracted attention in nanomedicine due to its antioxidant and anticancer activity, biocompatibility, and physicochemical properties [11, 12]. SeNPs have emerged as a novel form of Se due to their unique properties and have displayed increased biocompatibility and bioavailability, which is comparable to other inorganic nanocarriers [13, 14]. Although much research has been focused on the above NPs, interest in using transition metals, such as palladium (Pd), is growing due to their high surface area to volume ratio and surface energy, making them desirable as potential catalysts [15, 16]. PdNPs can be easily conjugated to biomolecules and, together with their catalytic activity, allow their use as biosensors. PdNPs are also reported to be non-toxic at low concentrations, favouring their use as anti-tumour, antimicrobial, and photothermal agents [17].

Although inorganic NPs exhibit great potential for biomedical applications, in most cases, they cannot directly bind to specific biomolecules and can also be thermodynamically unstable, resulting in aggregation. This can be overcome by functionalization of the NPs with suitable polymers [18]. Commonly used polymers in nanomedicine include poly-L-lysine (PLL), polyethyleneimine (PEI), and chitosan (CS). PLL is biodegradable and comprises 25-30 L-lysine residues with an ε-amino group and α-carboxyl linkages, which imbue properties to PLL such as high stability and water solubility, which reduce its potential toxicity. Hence, it has been considered non-toxic [19, 20]. Due to its cationic nature, it can penetrate cancer cells and is highly effective in inhibiting cell development by attaching and binding tightly to the cell membrane [21]. PEI consists of repeating amino groups and two branched carbon aliphatic spacers and can exist as either a linear or branched chained polymer [22]. PEI possesses pH buffering properties in the endosome, which can destabilize the vesicle and encourage the cytoplasmic conveyance of the endocytosed molecules [23]. CS is a derivative of chitin that is commonly found in the exoskeletons of crustaceans. It contains D-glucosamine and N-acetyl-D-glucosamine that are linked by a glycosidic β-(1-4) bond [24]. CS displays high levels of biocompatibility, biodegradability, minimal immunogenicity, and low cytotoxicity [25]. These polymers are widely used in cancer therapy research due to their cationic nature, making them ideal functionalization agents of NPs providing stability and conjugation with therapeutic agents such as anticancer drugs and nucleic acids, allowing for their safe and efficient delivery to cancer cells.

The application of inorganic NPs and polymers has not been fully exploited due to concerns about their potential cytotoxicity *in vivo*. However, before any animal-based studies, *in vitro* investigations are crucial. Hence the study at hand characterized and evaluated the *in vitro* cytotoxicity of four inorganic NPs (AuNP, AgNP, PdNP, and SeNP) and three polymers (PLL, PEI, and CS), which are commonly used in nanomedicine.

MATERIALS AND METHODS

Materials

Gold (III) chloride (HAuCl$_4$, Mw: 339.785 g.mol^{-1}), palladium (II) chloride (PdCl$_2$, Mw: 177.33 g.mol^{-1}), silver nitrate (AgNO$_3$, Mw:169.87 g/mol), sodium selenite (Na$_2$SeO$_3$, Mw: 172.94 g.mol^{-1}), poly- L-lysine (PLL, Mw: 84 kDa), polyethyleneimine (PEI, Mw: 25 kD), chitosan (CS, 75% - 85% deacetylated), ascorbic acid (C$_6$H$_8$O$_6$, Mw: 176.12 g.mol^{-1}), phosphate-buffered saline (PBS) tablets

and dialysis tubing (MWCO = 12 kDa) were purchased from Sigma Aldrich (St. Louis, MO, U.S.A). Trisodium citrate ($Na_3C_6H_5O_7$, Mw: 258.06 g.mol^{-1}), sodium borohydride ($NaBH_4$, Mw: 37.83 g.mol^{-1}), 3-(4,5-dimethylthiazol-2-yl)-2,5-diphenyl tetrazolium bromide (MTT) salt, dimethylsulfoxide (DMSO), acridine orange hemi (zinc chloride) salt [3,6-Bis (dimethylamino) acridine hydrochloride zinc chloride double salt] ($C_{17}H_{19}N_3$, Mw: 265.36 g.mol^{-1}), and ethidium bromide (EB) were purchased from Merck (Darmstadt, Germany). The human embryonic kidney (HEK293), cervical carcinoma (HeLa), hepatocellular carcinoma (HepG2), and breast adenocarcinoma (MCF-7) cell lines were initially procured from the American Type Culture Collection (ATCC) (Manassas, USA). Eagle's minimum essential medium (EMEM) containing L-glutamine (4.5 g.L^{-1}), trypsin-EDTA mixture [Versene (EDTA) 200 mg. L^{-1} and Trypsin 170.000 U L^{-1}] and antibiotics (100×) containing penicillin G (10 000 U mL^{-1}), streptomycin sulfate (10000 µg. mL^{-1}) and amphotericin B (25 µg. mL^{-1}) mixtures were purchased from Lonza BioWhittaker (Verviers, Liège, Belgium). Fetal bovine serum (FBS) was purchased from HyClone Laboratories (Inc, Utah, USA.) All sterile tissue culture plastic consumables were obtained from Corning Incorporated (Corning, NY, USA). All other chemicals and reagents were of analytical purity grade or higher and purchased commercially. Ultrapure deionized 18 MOhm water (Milli-Q50) was used in all preparations.

Gold nanoparticle (AuNP) synthesis

Colloidal AuNPs were synthesized using the Turkevich method, as previously described [7]. Approximately 28 ml of 18 MOhm water was heated to 90 °C for two minutes, followed by the addition of 375 µl HAuCl$_4$ (0.03 M) under constant heating and stirring. After that, 1 ml of 1% trisodium citrate was added, and a progressive colour change from dark blue to deep red was observed. The AuNP solution was then stirred for 10 minutes, cooled, and the final AuNP product (0.08 µg/µl) was stored at room temperature.

Silver nanoparticle (AgNP) synthesis

AgNPs were synthesized using a previously described method [26]. Approximately 50 ml of distilled water was heated to 95 °C. To this was added 8.5 mg of silver nitrate (AgNO$_3$) with stirring for 10 minutes. After that, 1 ml of 1% trisodium citrate was added dropwise, and the resulting solution was removed from the heat and stirred until the suspension reached room temperature. The AgNPs were stored at room temperature in the dark.

Selenium nanoparticles (SeNP)

SeNPs were synthesized using the precipitation method described in the literature [6]. A 1 mM ascorbic acid solution was added dropwise to a 0.013 M sodium selenite solution and stirred at room temperature. The volume was then adjusted to 25 ml with 18 MOhm water. The solution was stirred for 1 hour and was then dialyzed against 18 MOhm water to remove any unreacted material. The final SeNP solution (0.07 µg/µl) was stored at 4 °C.

Palladium nanoparticles (PdNP)

PdNPs were synthesized using an adapted two-step process as reported in the literature [27, 28]. The first step involved the synthesis of dihydrogen tetrachloropalladate (H$_2$PdCl$_4$). Approximately 35.6 mg palladium (II) chloride (PdCl$_2$) was added to 2.4 ml of HCl (0.2 M) and 100 ml of 18 MOhm water and stirred for 1 hour. The solution was refluxed for 3 hours and aged for 2 days away from light to produce a pale-yellow H$_2$PdCl$_4$ (2 mM) solution. To 5 ml of H$_2$PdCl$_4$ was added 5 ml of 18 MOhm water with stirring for 10 minutes. Thereafter, 108 µl SDS (100 mM) was added, followed by the immediate addition of cold sodium citrate (100 mM) with stirring for 1 minute. Thereafter, 15 µl of cold NaBH$_4$ (100 mM) was added, changing the color from pale yellow to dark brown. The solution was stirred for 10 minutes before 15 µl NaBH$_4$ was added, and the mixture was stirred on ice for 1 hour. The final PdNP solution was stored in a dark bottle at 4 °C.

Characterisation

The absorbance spectra of the synthesized NPs were determined using UV-visible spectroscopy over a wavelength range of 200-800 nm (JASCO-V-730 bio-spectrophotometer, Japan). The absorption maxima for each NP preparation were recorded.

The ultrastructural morphology of the polymers and NPs was determined using transmission electron microscopy (TEM). Before visualization, the polymers were negatively stained with uranyl acetate. The polymers and NPs were viewed using a JEOL JEM-2100 electron microscope (JEOL, Tokyo, Japan), and the images were captured using Soft Imaging System Megaview III (Olympus Corporations, Münster, Germany).

The hydrodynamic size and zeta potential were evaluated using nanoparticle tracking analysis (NTA) in a Nanosight NS500 (Malvern, Worcestershire, UK) at 25 °C. Videos were recorded and analyzed with the inbuilt NTA 3.2 software.

Cell culture

Cell culture protocols were carried out under sterile conditions in a Class II Biosafety laminar flow hood. Four cell lines were chosen for the study, namely, the embryonic kidney (HEK293), which served as the non-cancer control cell line, cervical carcinoma (HeLa), breast adenocarcinoma (MCF-7), and hepatocellular carcinoma (HepG2) cell lines. All cells were grown in a humidified 37 °C incubator as adherent cultures and maintained in 25 cm^2 tissue culture flasks containing 5 ml complete medium (EMEM) containing 10% ($^v/_v$) FBS, and 1% ($^v/_v$) antibiotic (100 U/ml penicillin, 100 μg/ml streptomycin, 0.25 μg/ml amphotericin). Cells were routinely trypsinized upon confluency and were either sub-cultured, cryopreserved, or seeded into multi-well plates for cell-based assays. All cell-based assays were conducted in triplicate.

Cytotoxicity assay

The 3-(4,5-dimethylthiazol-2-yl)-2,5-diphenyl tetrazolium bromide (MTT) assay was used to evaluate any possible toxicities associated with the chosen polymers and inorganic NPs. Cells were trypsinized once confluency was reached and seeded into 96 well plates at densities of 3.8 $\times 10^4$ cells/well, followed by incubation at 37 °C overnight. Thereafter, the spent medium was replaced with 100 μl fresh complete medium. The inorganic NPs and polymers (5- 20 μg/ml) were introduced into their respective wells and were incubated for 48 hours at 37 °C. The assay was conducted in triplicate. Following incubation, the medium was removed, and 100 μl serum-free medium containing 10 μl MTT reagent (5 mg/ml in PBS) was added to the wells and incubated for 4 hours at 37 °C. The medium/MTT mixture was then removed, and 100 μl DMSO was introduced into the respective wells to solubilize the resulting formazan crystals. Control wells containing untreated cells were treated similarly. Absorbance was measured at 570 nm against a DMSO blank using a Mindray MR-96A microplate reader (Vacutec, Hamburg, Germany). The cell viabilities were determined using the equation below:

$$\text{Cell Viability (\%)} = (\text{OD}_{\text{treated cells}} / \text{OD}_{\text{control cells}}) \times 100$$

Apoptosis assay

The acridine orange/ethidium bromide (AO/EB) dual staining method was used to evaluate induced apoptosis quantitatively. The cell lines and concentrations of the polymers and inorganic NPs in which > 25% cell death was achieved in the MTT assay were evaluated. Cells were seeded at densities of 2.6 $\times 10^4$ cells/well in 48 well plates containing 0.25 ml medium and incubated at 37 °C overnight. After that, the medium was replaced with fresh medium, followed by the addition of the polymers and inorganic NPs into their respective wells, as outlined in Table 1. Untreated cells were included as a control. Following incubation for 24 hours, the medium was removed, and the cells were washed twice with PBS. Thereafter, 10 μl of AO/EB dye (0.1 mg/ml:0.1 mg/ml in PBS) was added to the cells and incubated at room temperature for 5 minutes. The cells were then washed with PBS to remove unabsorbed dye and viewed under an Olympus fluorescence microscope. Images were captured using a CC12 fluorescence camera and AnalySIS software (Olympus Soft Imaging Solutions, Olympus, Japan) at 20 × magnification. Apoptotic indices (AI) were determined using the following equation:

$$\text{Apoptotic Index} = \text{number of apoptotic cells} / \text{total number of cells}$$

Statistical analysis

Data are presented as a mean ± standard deviation (SD n=3). Data was analyzed using GraphPad Prism version 6 software (GraphPad Software Inc., La Jolla, CA, USA). Statistical analysis between means was evaluated using a two-way analysis of variance (ANOVA) followed by Dunnett's multiple groups

mean comparison test. p values < 0.05 were considered significant.

RESULTS AND DISCUSSION

Nanoparticle and polymer characterization

The UV-visible spectra of the synthesized NPs are presented in Figure 1. The AuNP, AgNP, and SeNP exhibited distinct peaks at 518 nm, 456 nm, and 285 nm, respectively, with the PdNP producing a much lower absorbance with minor peaks at 350 nm, 375 nm, and 405 nm. These results correlate with

those described in the literature and confirm the synthesis and presence of the NPs [29-32]. Visually, the final colour of the respective NP preparations further confirmed the presence of the synthesized NPs.

The ultrastructural characteristics of the NPs and polymers from TEM are shown in Figure 2. All NPs (Figure 2A) exhibited spherical morphologies with slight aggregation. Previous reports have suggested that aggregation of NPs occurs to minimize surface energies to achieve the lowest energy state [33-35]. TEM micrographs showed the variations

Table 1. Concentrations of the nanoparticles and polymers (µg/ml) used in the apoptosis assay.

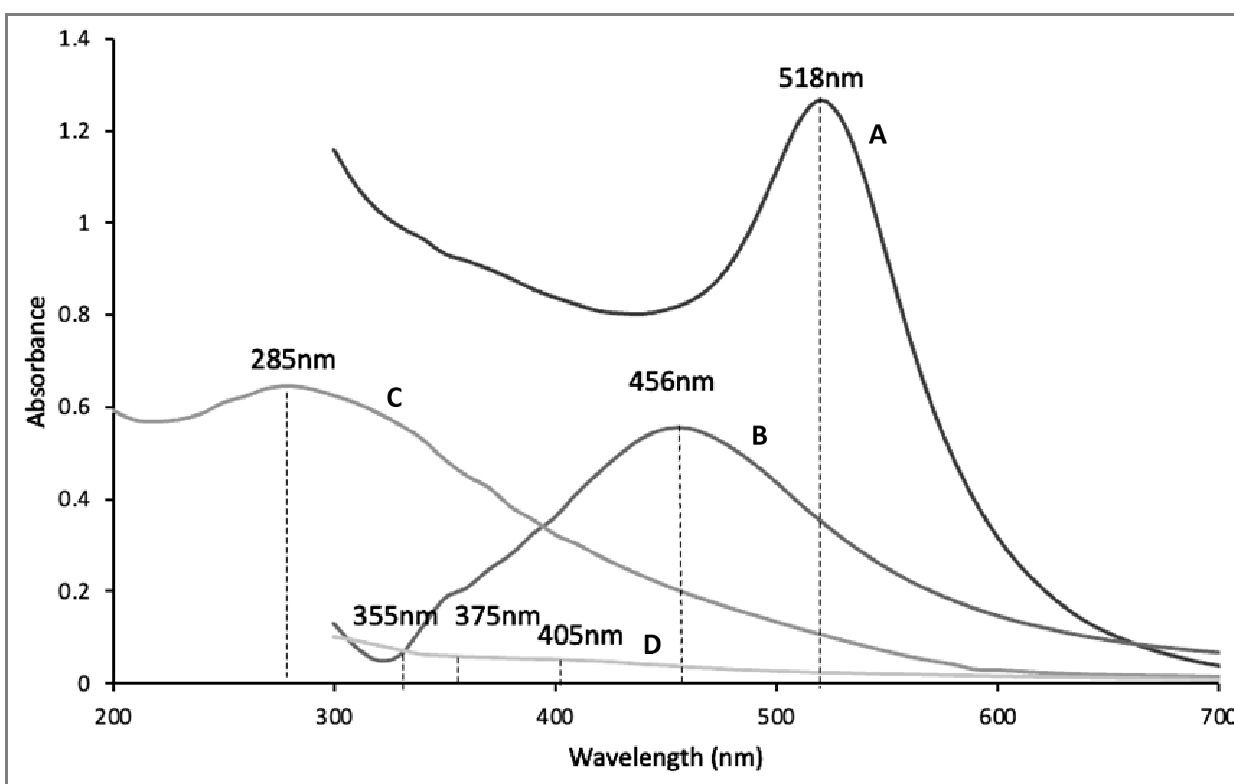| Cell Lines	AgNP (µg/ml)	SeNP (µg/ml)	PLL (µg/ml)	PEI (µg/ml)	CS (µg/ml)
HEK293	20	-	-	-	-
HeLa	20	20	-	20	-
HepG2	-	20	5	5	5
MCF-7	20	20	-	-	-

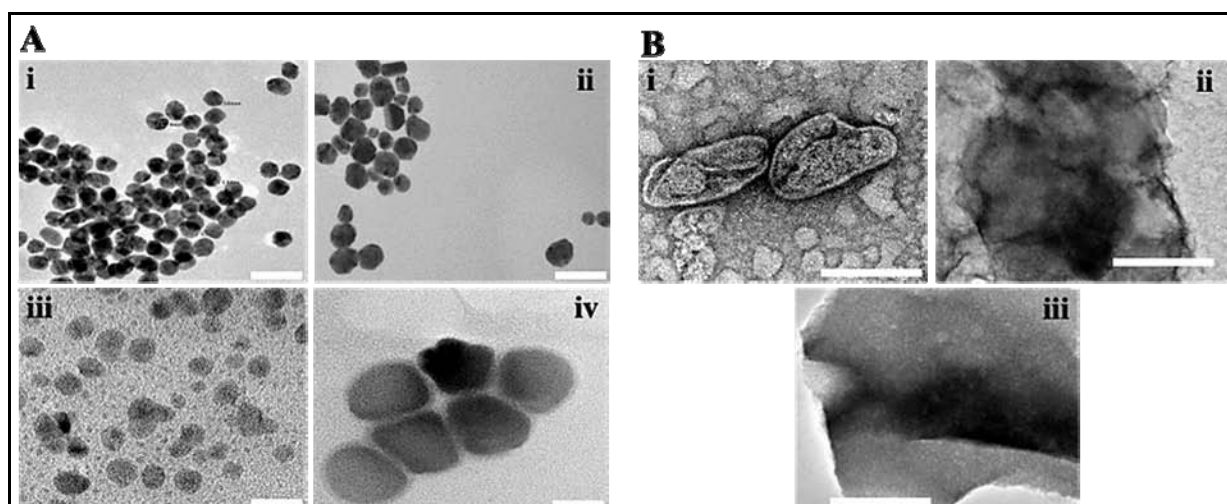**Figure 1.** UV-visible spectra of (A) AuNPs, (B) AgNPs, (C) SeNPs, and (D) PdNPs.

Figure 2. TEM micrographs of (A) Nanoparticles and (B) Polymers. **A**: (i) AuNP, (ii) AgNP, (iii) PdNP and (iv) SeNP. **B**: (i) PLL, (ii) PEI and (iii) CS. Scale Bars = 50 nm for **A** (iii), 100 nm for A (i, ii and iv) and 200 nm for **B** (i-iii).

Table 2. Hydrodynamic size, zeta potential, and polydispersity indices of inorganic nanoparticles and polymers.

Nanoparticle/ Polymer	Hydrodynamic Size (nm) Mean ± SD (n=5)	Zeta Potential (mV) Mean ± SD (n=5)	Polydispersity Index (PDI)
AuNP	68.9 ± 2.5	- 7.8 ± 3.7	0.001
AgNP	64.9 ± 0.6	- 4.4 ± 0.8	0.000009
PdNP	85.5 ± 20	- 4.6 ± 0.8	0.055
SeNP	71.8 ± 3.9	-13.3 ± 0.4	0.0029
PLL	92.4 ± 46.9	20.2 ± 0.5	0.26
PEI	150.1 ± 14.8	42.3 ± 2.0	0.0097
CS	193.8 ± 50.2	48.8 ± 6.8	0.067

in polymer shape, with PLL being oval, PEI being spherical, and CS appearing irregular and as a film (Figure 2B). These observations are consistent with those reported in the literature [36-38].

The hydrodynamic diameters and zeta potentials of the NPs and polymers, as determined by NTA, are presented in Table 2. The polymers appear to be much larger than the NPs; however, they all fall within the nanometer range (< 200 nm), which is desirable for biomedical applications [39]. The zeta potential indicates the colloidal stability, with values < -25 mV or > + 25 mV being considered stable. As seen in Table 2, all the NPs exhibited low levels of stability, which is commonly seen for inorganic NPs that are not functionalized [40].

This further supports the need for NP functionalization for stabilization. The inorganic NPs all possessed a negative charge, suggesting that anions are present on their surfaces [41, 42]. In contrast, the polymers were very stable with zeta potentials greater than + 20 mV, especially PEI and CS. This makes them ideal candidates for the functionalization and stabilization of the NPs. Furthermore, the positive charge associated with the polymers supports their encapsulation of the therapeutic agent (nucleic acid or chemotherapeutic drug) through electrostatic interactions, resulting in a nanocomplex that can be safely delivered to diseased cells. In addition, the conformation of these polymers also enables the entrapment of biomolecules within their chain network.

The size distribution of NPs is represented by the polydispersity index (PDI), where indices lower than 0.1 represent a monodisperse size population. In contrast, indices as high as 0.4 indicate a polydisperse sample with a higher tendency of agglomeration [43]. All the NP preparations, as well as PEI and CS, exhibited low PDI values (< 0.1) (Table 2), which indicates their uniformity in size and monodisperse nature. PLL exhibited a slightly higher PDI, suggesting that the sample was somewhat more polydisperse.

In vitro cytotoxicity

Cytotoxicity is one of the biggest hurdles in the clinical application of NPs and polymers in nanomedicine, making it crucial to evaluate any associated cytotoxicity [44]. The colorimetric MTT assay, which measures the reduction of yellow 3-(4,5-dimethylthiazol-2-yl)-2,5-diphenyl tetrazolium bromide (MTT) to a purple formazon product by mitochondrial reductase, was used [45]. Therefore, this reduction can only occur in viable cells and is a direct measure of cell viability. The cytotoxicity of the NPs and polymers is shown in Figure 3.

Cytotoxicity was investigated in four human cell lines, namely, HEK293, HeLa, MCF-7, and HepG2.

All NPs, apart from the AgNPs, were well tolerated in the HEK293 cells (Figure 3A) with cell viability ≥ 70%. This indicates that these NPs and polymers are biocompatible and will not adversely affect the renal system. In addition, HEK293 cells have been commonly used as control normal cells, which suggests that in cancer treatment, normal cells will not be adversely affected by these NPs. AgNPs showed moderate toxicity in the HEK293 cells (30.46% cell death), with more significant toxicity in the HeLa (98.8% cell death) and the MCF-7 (99.5% cell death) cells at the highest concentration tested. Toxicity associated with AgNPs could be due to the large variations in their physicochemical characteristics, including particle size, surface chemistry, and shape. There have been many reports on the associated cytotoxicity of AgNPs, with the consensus being that the mitochondria are the primary target of Ag^+. In the presence of Ag^+, proteinaceous pores form in the mitochondrial membrane, which could result in swelling, aberrant metabolism, and, finally, apoptosis. Furthermore, cell death in the presence of AgNPs can be due to oxidative stress, DNA damage, and the regulation of cytokine production [46]. Cellular uptake of AgNPs leads to the production of radical oxygen
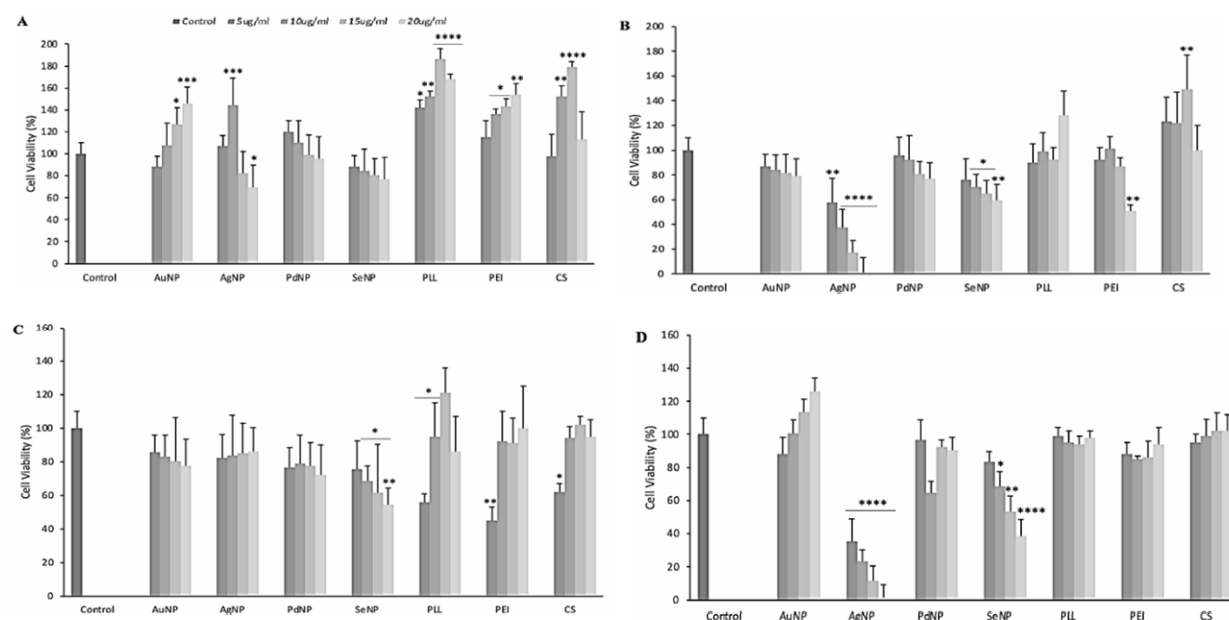

Figure 3. Cytotoxicity profile of nanoparticles and polymers (µg/ml) in (A) HEK293, (B) HeLa, (C) HepG2 and (D) MCF-7 cells. Data are presented as means ± SD (n = 3), where * $p ≤ 0.05$, ** $p ≤ 0.01$, *** $p ≤ 0.001$ and **** $p ≤ 0.0001$ are considered to be statistically significant vs the control.

species (ROS), which, in turn, results in oxidative stress. ROS produced in high amounts can result in cell death due to apoptosis or necrosis [47-51]. Due to the strong optical extinctions of AgNPs at visible wavelengths, they can interfere with colorimetric assays such as the MTT assay used in this study. Since the mitochondria is a primary target of AgNPs, and the MTT assay measures cell viability based on cellular mitochondrial activity, there may be a need to evaluate the toxicity of AgNPs further to confirm their mechanism of action and if cell death is due to necrosis or induced apoptosis.

The SeNPs were well-tolerated by the HEK293 cells; however, greater cell death was evident in the HeLa (40.79%), HepG2 (45.5%), and MCF-7 (61.5%) cells. Previous studies have shown the remarkable anticancer activity of SeNPs due to their ability to inhibit cancer cell growth by inducing cell cycle arrest at the S-phase through deregulation of the eIF3 protein complex [52]. SeNPs are known to possess the ability of selectivity between normal and cancer cells, which is supported by the results of this study where the SeNPs showed minimal toxicity to the normal HEK293 cells (> 75% cell viability) while inducing cell death in the cancer cells tested. Selective cellular uptake of SeNPs by cancer cells can occur by endocytosis, which causes cellular apoptosis by triggering apoptotic signal transduction pathways [52]. Several mechanisms have been proposed to describe the anticancer activity of selenium, including apoptosis, cell multiplication restraint, and redox state regulation. From these, the most consideration is given to apoptosis as the fundamental cancer chemoprevention by seleno species [53-55].

All polymers were well tolerated by the HEK293 and MCF-7 cells, with cell viability exceeding 85% (Figure 3A and D), attesting to the biocompatible nature of these polymers. However, PEI was the least tolerated in the HeLa and HepG2 cell lines, with 55.96% and 62.4% cell viability, respectively. There are two mechanisms by which PEI elicits toxicity. The first mechanism involves the disruption of the plasma membrane, which redistributes phosphatidylserine, resulting in the activation of caspase-3 and immediate cell death. The second mechanism disrupts the mitochondrial membrane

due to the formation of divots in the outer mitochondrial layer, which allows for translocation of caspase-3 and cytochrome c discharge, resulting in delayed cell death [56].

Interestingly, PLL and CS exhibited cytotoxicity in the HepG2 cells with viabilities of 55.96% and 62.4%, respectively. It has been noted that PLL can cause cytochrome c release from the mitochondrial membrane, resulting in swelling. It is also involved in releasing an assortment of cellular and protein kinases, resulting in cell death due to the signaling and activation of protein kinases [56]. CS can inhibit proliferation of liver cancer cells by penetrating the cell membrane and inducing lipid peroxidation [57].

Overall, AuNP, PdNP, SeNP, and all the polymers studied show great potential in nanomedicine for cancer therapy, showing little to no toxicity to the HEK293 cell line, providing evidence of their safe, biocompatible nature.

Apoptosis assay

Apoptosis is organized cell death in response to biochemical events that result in cell morphology changes, including membrane blebbing, cell shrinkage, nuclear fracture, chromatin precipitation, and chromosomal DNA dissociation [58]. The dual AO-EB staining method distinguishes between normal apoptotic (early and late stages) and necrotic cells because differential staining will occur between the cells. A green fluorescence will be emitted by AO-stained viable cells, with a yellow-to-red fluorescence exhibited by EB-stained cells due to compromised membranes [26]. The fluorescence images (Figure 4) and apoptotic indices (Table 3) show that the control (untreated) cells were all viable and did not exhibit any signs of apoptosis. The HEK293 cells treated with the AgNPs (Figure 4A ii) showed visible changes to their morphology and appeared more rounded and appeared to be in the early apoptotic stage. The MCF-7 cells treated with AgNPs and SeNPs appeared to be in the late stages of apoptosis due to the changes in the cell morphology and compromised chromatin (Figure 4B ii and iii). However, from the apoptotic indices, there is a larger cell population in this phase of apoptosis following treatment with AgNPs when compared to SeNPs, which corroborates the results from the MTT
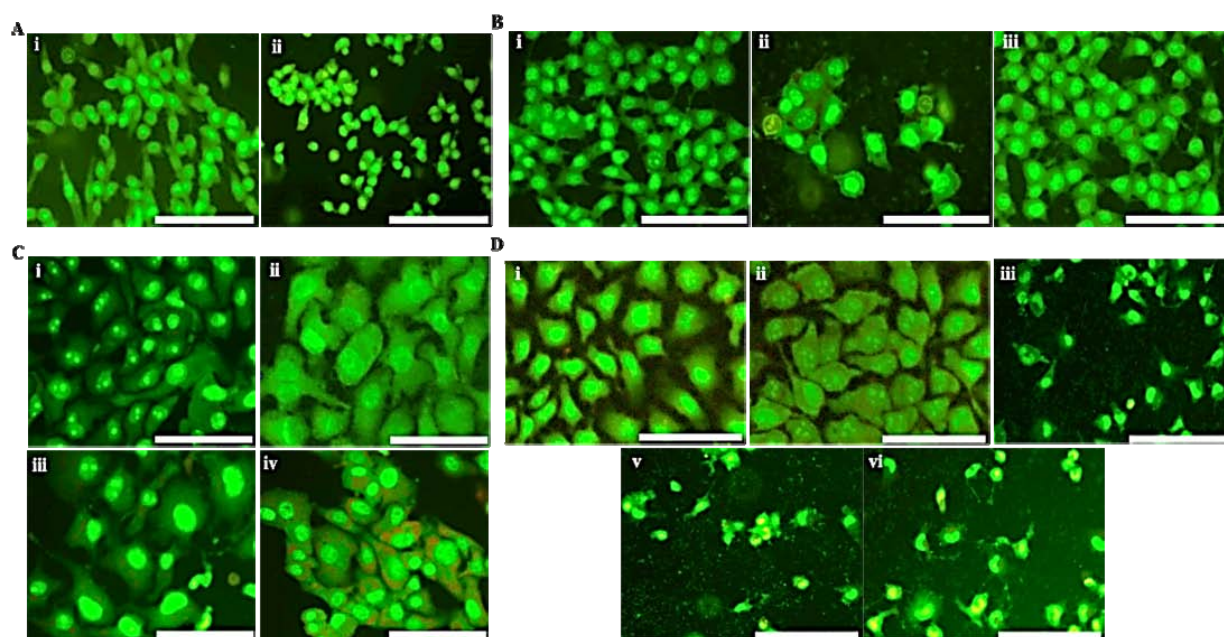
Figure 4. Fluorescent images of (A) HEK293, (B) MCF-7, (C) HeLa and (D) HepG2 cell lines following AO/EB staining. **A**: (i) Control and (ii) AgNP. **B**: (i) Control, (ii) AgNP and (iii) SeNP. **C**: (i) Control, (ii) AgNP, (iii) SeNP and (iv) PEI. **D**: (i) Control, (ii) SeNP (iii) PLL, (iv) PEI and (v) CS. Scale bar = 100 μm.

Table 3. Apoptotic indices of cells treated with inorganic nanoparticles and polymers.

Cell Lines	AgNP	SeNP	PEI	PLL	CS
HEK293	0.09	-	-	-	-
HeLa	0.28	0.1	0.34	-	-
HepG2	-	0.09	0.32	0.4	0.28
MCF-7	0.65	0.05	-	-	-

assay. HeLa cells treated with AgNPs, SeNPs, and PEI (Figure 4C ii-iv) exhibited some red fluorescence, which indicates cells with compromised membranes in the late stages of apoptosis. The MTT assay revealed that the HepG2 cells were the most affected by treatment with SeNPs and polymers with cell viability < 75%. The apoptosis assay confirmed that the HepG2 cells treated with the SeNPs were in the late apoptotic stage (Figure 4D ii). However, cells treated with polymers exhibited extreme changes to their morphology, including cell shrinkage and condensed chromatin, which indicates cells in the late apoptotic stage (Figure 4D iii-v). Overall, cells treated with the NPs and polymers did not show signs of necrosis resulting from cell injury due to internal or external stresses, with most cell death occurring due to apoptosis.

CONCLUSION

Assessing the cytotoxicity of NPs and polymers is essential to ascertain their potential use for biomedical applications. The results of this study revealed the AuNPs and PdNPs exhibited minimal toxicity in all cells tested, suggesting that they are ideal candidates for use in nanomedicine, especially as gene or drug delivery vehicles. The anticancer activity associated with SeNPs was proven in this study. These NPs induced cell death in the three cancer cells tested, with minimal toxicity in the non-cancer HEK293 cells. A similar trend was noted for the cationic polymers, confirming their biocompatibility for biomedical applications. AgNPs, however, did possess cytotoxicity in the HEK293 cells, with the apoptosis assay confirming that this was due to the onset of apoptosis. The AgNPs

were better tolerated by the HepG2 cells, suggesting that these NPs may be cell-specific and further studies are needed if they are to be considered in therapeutics. Modifications with polymers may be necessary to reduce toxicity in normal cells. The polymers tested can be used to functionalize these NPs and other inorganic NPs for better stability and biocompatibility. This study has provided evidence for using some of these inorganic NPs and polymers in nanomedicine and can pave the way for designing suitable therapeutic delivery vehicles for cancer therapy.

ACKNOWLEDGEMENTS

CONFLICT OF INTEREST STATEMENT

The authors declare no conflict of interest.

REFERENCES

1. Bray, F., Ferlay, J., Soerjomataram, I., Siegel, R. L., Torre, L. A. and Jemal, A. 2018, CA: Cancer J. Clin., 68, 394.
2. Venkatas, J. and Singh, M. 2023, Nanomedicine, 18 (13), 945.
3. Misra, R., Acharya, S. and Sahoo, S. K. 2010, Drug Discov., 15(19), 842.
4. Gmeiner, W. H. and Ghosh, S. 2014, Nanotechnol. Rev., 3(2), 111.
5. McNamara, K. and Tofail, S. A. M. 2017, Adv. Phys., 2(1), 54.
6. Pillay, N. S., Daniels, A. and Singh, M. 2020, Int. J. Mol. Sci., 21, 7177.
7. Joseph, C., Daniels, A., Singh, S. and Singh, M. 2022, Pharmaceutics, 14, 53.
8. Akinyelu, J. and Singh, M. 2019, Appl. Nanosci., 9(1), 7.
9. Nedelcu, I-A., Ficai, A., Sonmez, M., Ficai, D., Oprea, O. and Andronescu, E. 2015, Curr. Org. Chem., 18(2), 173.
10. Tyagi, P. K., Mishra, R., Khan, F., Gupta, D. and Gola, D. 2020, Biointerface Res. Appl. Chem., 10(6), 6587-6596.
11. Xia, J., Li, T., Lu, C. and Xu, H. 2018, Macromolecules, 51, 7435.
12. Maiyo, F. and Singh, M. 2017, Nanomedicine, 12, 1075.
13. Naidoo, S., Daniels, A., Habib, S. and Singh, M. 2022, Int. J. Mol. Sci., 23, 1492.
14. Ferro, C., Florindo, H. F. and Santos, H. A. 2021, Adv. Healthcare Mater., 10, 2100598.
15. Cookson, J. 2012, Platin. Met. Rev., 56(2), 83.
16. Leso, V. and Iavicoli, I. 2018, Int. J. Mol. Sci., 19(2), 503.
17. Dumas, A. and Couvreur, P. 2015, Chem. Sci., 6, 2153.
18. Li, D. and Kaner, R. B. 2006, J. Am. Chem. Soc., 128, 968.
19. Sitterley, G. 2008, BioFiles, 3(8), 12.
20. Shukla, S. C., Singh, A., Pandey, A. K. and Mishra, A. 2012, Biochem. Eng. J., 65(1), 70.
21. Debnath, S., Karan, S., Debnath, M., Dash, J. and Chatterjee, T. K. 2017, Asian Pac. J. Cancer Prev., 18(8), 2255.
22. Yemul, O. and Imae, T. 2008, Colloid Polym. Sci., 286(6-7), 747.
23. Nishikawa, M., Kawakami, S., Yamashita, F. and Hashida, M. 2003, Methods Enzymol., 373, 384.
24. Sánchez-Machado, D. I., López-Cervantes, J., Correa-Murrieta, M. A., Sánchez-Duarte, R. G., Cruz-Flores, P. and de la Mora-López, G. S. 2019, Nonvitamin and Nonmineral Nutritional Supplements, M. Nabavi, and A. S. Silva, (Eds.), Elsevier, Academic Press, 485.
25. Lizardi-Mendoza, J., Argüelles Monal, W. M. and Goycoolea Valencia, F. M. 2016, Chitosan in the Preservation of Agricultural Commodities, S. Bautista-Baños, G. Romanazzi, and A. Jiménez-Aparicio, (Eds.), Elsevier, Academic Press, 3.
26. Veerappan, R., Daniels, A. and Singh, M. 2021, Int. J. Nanosci., 20(5), 2150041.
27. Shanthi, K., Vimala, K., Gopi, D. and Kannan, S. 2015, RSC Adv., 5, 44998.
28. Chen, D., Li, J., Cui, P., Liu, H. and Yang, J. 2016, J. Mater. Chem. A, 4, 3813.
29. Link, S. and El-Sayed, M. A. 1999, J. Phys. Chem., 103(21), 4212.
30. Singh, J., Bajaj, R., Harpreet, K., Harjot, K. and Navneet, K. 2016, J. Nanomed. Res., 4(3), 00092.
31. Yang, X., Li, Q., Wang, H., Huang, J., Lin, L., Wang, W. and Jia, L. 2009, J. Nanoparticle Res., 12(5), 1589.

32. Chudobova, D., Cihalova, K., Dostalova, S., Ruttkay-Nedecky, B., Rodrigo, M., Tmejova, K., Kopel, P., Nejdl, L., Gumulec, J.K., Krizkova, S., Kynicky, J., Kizek, R. and Adam, V. 2014, FEMS Microbiol. Lett., 351(2), 195.

33. Dubey, S. P., Lahtinen, M. and Sillanpää, M. 2010, Process Biochem., 45(7), 1065.

34. Nadagouda, M. N. and Varma, R. S. 2008, Green Chem., 10(8), 859.

35. Tran, P. A. and Webster, T. J. 2011, Int. J. Nanomedicine, 6(2011), 553.

36. Zhang, X., Oulad-Abdelghani, M., Zelkin, A. N., Wang, Y., Haîkel, Y., Mainard, D., Jean- Claude, V., Caruso, F. and Benkirane-Jessel, N. 2010, Biomaterials, 31(7), 1699.

37. Liu, X., Mo, Y., Liu, X., Guo, R., Zhang, Y., Xue, W., Zhang, Y., Wang, C. and Ramakrishna, S. 2016, Mater. Sci. Eng. C Mater. Biol. Appl., 62, 177.

38. Jiang, H., Su, W., Caracci, S., Bunning, T. J., Cooper, T. and Adams, W. W. 1996, J. Appl. Polym. Sci., 61(7), 1169.

39. Oladimeji, O., Akinyelu, J., Daniels, A. and Singh, M. 2021, Int. J. Mol. Sci., 22, 5072.

40. Xu, L., Liang, H.W., Yang, Y. and Yu, S.H. 2018, Chem. Rev., 118(7), 3209.

41. Gangadoo, S., Stanley, R., Hughes, O. J., Moore, R. J. and Chapman, J. 2017, Inorg. Nano-Metal Chem., 47, 1568.

42. Singh, D. and Singh, M. 2021, Pharmaceutics, 13 (3), 298.

43. Clayton, K. N., Salameh, J. W., Wereley, S. T. and Kinzer-Ursem, T. L. 2016, Biomicrofluidics, 10, 054107.

44. Lewinski, N., Colvin, V. and Drezek, R. 2008, Small, 4(1), 26.

45. Mosmann, T. J. 1983, Immunol. Meth., 65, 55.

46. Stensberg, C. M., Wei, Q., McLamore, E. S., Porterfield, D. M., Wei, A. and Sepúlveda, M. S. 2011, Nanomedicine, 6(5), 879.

47. Hussain, S. M., Hess, K. L., Gearhart, J. M., Geiss, K. T. and Schlager, J. J. 2005, Toxicol. In Vitro, 19, 975.

48. Almofti, M. R., Ichikawa, T., Yamashita, K., Terada, H. and Shinohara, Y. 2003, J. Biochem., 134, 43.

49. Wang, M. G., Katayama, H. and Ohgaki, S. 2007, Water Res., 41, 4097.

50. Carlson, C., Hussain, S. M., Schrand, A. M., Braydich- Stolle, L. K., Hess, K. L., Jones, R. L. and Schlager, J. J. 2008, J. Phys. Chem. B, 112, 13608.

51. Asharani, P. V., Kah, G. L. K., Hande, M. P. and Valiyaveettil, S. 2009, ACS Nano, 3, 279.

52. Hosnedlova, B., Kepinska, M., Skalickova, S., Fernandez, C., Ruttkay-Nedecky, B., Peng, Q., Baron, M., Melcova, M., Opatrilova, R., Zidkova, J., Bjørklund, G., Sochor, J. and Kizek, R. 2018, Int. J. Nanomedicine, 13, 2107.

53. Zhang, Y., Li, X., Huang, Z., Zheng, W., Fan, C. and Chen, T. 2013, Nanomedicine, 9(1), 74.

54. Wu, H., Zhu, H., Li, X., Liu, Z., Zheng, W., Chen, T., Yu, B. and Wong, K-H. 2013, J. Agric Food Chem., 61(41), 9859.

55. Pi, J., Jin, H., Liu, R., Song, B., Wu, Q., Liu, L., Jiang, J., Yang, F., Cai, H. and Cai, J. 2013, Appl Microbiol Biotechnol., 97(3), 1051.

56. Hunter, A. C. 2006, Adv. Drug Deliv. Rev., 58(14), 1526.

57. Adhikari, H. S. and Yadav, P. N. 2018, Int. J. Biomater., 2018, 2952085.

58. Brunelle, J. K. and Zhang, B. 2010, Drug Resist Update, 13(6), 172.